



ELSEVIER

Contents lists available at ScienceDirect

Journal of Luminescence

journal homepage: www.elsevier.com/locate/jlumin

Strain modulated defect luminescence in ZnO nanostructures grown on Si substrates

Hung-Ing Chen^a, Jui-Ju Hsiao^a, Yi-Jen Huang^a, Jen-Cheng Wang^a, Ya-Fen Wu^b,
Bing-Yuh Lu^c, Tzer-En Nee^{a,*}

^a Graduate Institute of Electro-Optical Engineering and Department of Electronic Engineering, Chang Gung University, 259 Wen-Hwa 1st Road, Kwei-Shan, Tao-Yuan 333, Taiwan, ROC

^b Department of Electronic Engineering, Ming Chi University of Technology, Taishan, New Taipei 243, Taiwan, ROC

^c Department of Electrical Engineering, Tun Gnan University, Shenkeng, New Taipei 222, Taiwan, ROC

ARTICLE INFO

Article history:

Received 4 February 2015

Received in revised form

13 July 2015

Accepted 1 August 2015

Available online 21 August 2015

Keywords:

ZnO nanostructure

Hydrothermal method

Defect luminescence

Strain modulated

ABSTRACT

The strain modulated defect green luminescence from ZnO nanostructures grown on silicon substrates has been investigated in-depth. According to the Warren–Averbach Fourier analysis of the X-ray diffraction profiles, both the internal strain and the average crystallite size of the well-ordered nano-size ZnO nanostructures could be subtly modulated by careful adjustment of the aqueous solution of zinc nitrate ($\text{Zn}(\text{NO}_3)_2$) and ammonium hydroxide (NH_3OH) used in the hydrothermal treatment. Visible defect-related and ultraviolet band-to-band emissions were characterized using temperature-dependent photoluminescence measurements over a broad temperature range from 20 to 300 K. It was found that the thermal-related tensile strain led to the blueshift of the green emission with increasing temperature, while the violet and ultraviolet emissions were thermally insensitive. These spectral observations were substantially corroborated by the deformation potential theory.

© 2015 Elsevier B.V. All rights reserved.

1. Introduction

Due to its unique properties, including high piezoelectricity, direct wide bandgap, large exciton binding energy, and high electron mobility, zinc oxide (ZnO) nanostructures are considered to be a candidate of priority for optoelectronic and nanowave device applications. Although the efforts for the fabrication of well-defined nanostructures are far reaching, it is surmised that the development of techniques for the preparation of novel nano-ZnO structures would be the most promising in the near future. Significantly, with respect to stoichiometric ZnO, it is worth noting that the potential role of crystalline imperfections that form in ZnO merits attention not only in fundamental defect science but also in defect engineering [1]. By virtue of the fact that the defect luminescence has importance in applications like the development of visible light sources [2], gas sensing [3], catalysis [4], cell-labeling [5], and high efficiency green phosphor [6], there has been a burgeoning of interest in the last decade in growth studies for the characterization of the green luminescence (GL) associated to oxygen vacancies in nanocrystalline ZnO [1,7,8].

Nano-ZnO has been synthesized by different methods, including metal–organic chemical vapor deposition (MOCVD) [9,10], physical vapor phase deposition [11–13], and the low temperature hydrothermal method [14–16]. The hydrothermal method, which involves heterogeneous nucleation in supersaturated solutions for the growth of nanostructures on the surface, has many advantages, being an easy procedure to implement requiring low temperature and pressure. From a practical point of view, this method is very simple, cost effective, nanoelectronic compatible, and suitable for large area substrates and results in the growth of ZnO films. As far as the defect radiations observed in ordered ZnO nanoarrays are concerned, many different techniques have been developed for the modulation of the defect-related transitions. The optical features of the deep-level states can be controlled by changing the radio-frequency (RF) magnetron sputtering conditions, including deposition time and RF power [17,18]. Furthermore, it has also been reported that the intrinsic defect emission intensity increases with an increase in the post-annealing temperature and increase of oxygen partial pressure [19]. Vertical self-aligned ZnO nanorods and nanotubes have a large surface coverage area and thus, the large amount of oxygen vacancies formed by atomic layer deposition with different cycle numbers exhibit strong photoluminescence (PL) [20]. These reports have shown that the growth or annealing conditions play major roles in the intrinsic characteristics of the nanocrystallines [8,16]. The optical properties of

* Corresponding author. Tel.: +886 3 2118800x5791; fax: +886 3 2118507.

E-mail address: neete@mail.cgu.edu.tw (T.-E. Nee).

deep level emissions in nanometer sized ZnO can be tailored through surface modification, impurity incorporation, annealing temperature and annealing atmosphere as well [21,22]. Due to the chemical reactions for the ZnO nanolattice fabricated by a hydrothermal process, it is expected to effectively modulate the micro-morphology of the nanostructures by adjusting the reaction parameters, as precursor concentration, pH, and forming time and temperature [14,15]. Generally, ammonium hydroxide (NH_4OH) introduced into the reaction system can deplete Zn ions at hydrothermal solutions, leading significantly to a great effect on suppression of the homogeneous ZnO nucleation [23]. Based on the principles of material thermodynamics, the formation energy determined the defect on the synthesis solutions. More recently, formalisms have been developed to use the total energy of the defect to calculate its concentration, under the assumption of thermodynamic equilibrium [24,25]. The formation energy of a point defect depends on the growth or annealing conditions in thermodynamic equilibrium and the concentration of an impurity, defect, or complex [26,27]. A formalism based on formation energies allows calculation of defect and impurity equilibrium structures and concentrations.

Many researchers have investigated the intense visible luminescences in ZnO arising from different defects, including oxygen vacancies (V_o), zinc vacancies (V_{Zn}), interstitials (Zn_i , O_i), and antisites (Zn_o , O_{Zn}) [8,11–13,16]. However, the origins of different defect emissions still lacked full understanding and more recent papers suggested that V_o in nonstoichiometric ZnO can have pronounced effects on the GL transition energy and intensity. Accurate knowledge of these equilibrium properties is of course essential not only for device engineering, but also from a physical point of view. Results from cathodoluminescence spectra as well as bimolecular recombination equations have revealed the characteristics of V_o in this GL [8]. Further studies are required to clarify the effects of the temperature, stress, electrical field, and magnetic field on the green emissions of ZnO [21,22,28]. Investigation of the two major possible mechanisms involved in the visible recombination processes, i.e., trap-state emissions and surface state emissions, has concentrated more on the spectral intensity. Mainly attributed to the thermal lattice dilation and electron–lattice interaction, the interband emission photon energy intrinsically followed the well-known Varshni formula [1]. Several studies have reported that the redshift with rising temperature for the UV emissions originally resulted from the bandgap shrinkage. However, anomalous temperature-dependent properties of the visible bands significantly differed from the bandgaps monotonically decreasing with increasing temperature. The blueshift with increasing temperature has been considered to be associated with the unique characteristics of the defect-related levels in the ZnO nanostructures. Essentially, since defect states that are different from the excitonic Bloch states are the localized ones; the defect luminescent energies originally emerged from the results of interactions of the surroundings on the orbital energy levels of a defect have been formulated by crystal field theory (CFT) [29]. The spectral observations associated with the nano-size effects on the strain were substantially assessed by the deformation potential theory. Furthermore, due to the profoundly complex nature of crystal field formulism, we believe that it is worthy to make considerable efforts to treat the defect transition energies in ZnO crystallines as model systems for quantum mechanical calculations. In fact, it has been shown that in single crystals the ultimate tensile strength and the yield strength scale with external sample size in a power law fashion, sometimes attaining a significant fraction of material's theoretical strength, and exhibiting the now-commonly-known phenomenon smaller are stronger thermal expanded coefficients.

Previously, we had reported that there were two paths for ZnO vacancy emissions resulting in strengthened peak energy when the measurement temperature increases [30,31]. Moreover, the surface plasmon resonance of aluminum cylindrical nanopillars formed on well-ordered ZnO has demonstrated an enhancement of the surface-defect related luminescence [1,7]. In the present work, ZnO nanostructures with engineered defects were synthesized on silicon substrates by the hydrothermal method with careful adjustment of the aqueous solution of zinc nitrate ($\text{Zn}(\text{NO}_3)_2$) and ammonia. The nanostructural properties of the samples were investigated, and the X-ray diffraction spectra were examined using Warren–Averbach Fourier analysis. Temperature-dependent photoluminescence measurements over a broad temperature range from 20 to 300 K provide insight into the roles of the thermally-induced strain in defect-related and ultraviolet (UV) band-to-band emissions. A good correlation was found between strain distribution and the luminescent spectra of the ZnO nanostructures.

2. Experimental procedure

The defects were investigated by examining the luminescence which was modulated by the strain in the ZnO nanostructures fabricated on a silicon substrate. A thin film of zinc acetate ($\text{Zn}(\text{CH}_3\text{COO})_2$) (comprised of a solution containing zinc acetate dihydrate ($\text{Zn}(\text{O}_2\text{CCH}_3)_2(\text{H}_2\text{O})_2$)) was spin coated onto the substrate and annealed at 300 °C in air for 20 min. The hydrothermal method was used to grow ZnO nanostructures on a Si substrate using an aqueous solution of zinc nitrate ($\text{Zn}(\text{NO}_3)_2$) and ammonium hydroxide (NH_3OH).

The samples were denoted as sample 1 (S1), sample 2 (S2), and sample 3 (S3), from smaller strain to larger strain. It was well-known that high pH environments inhibit the growth of nano-ZnO. The diameters of the nanowire-like ZnO were subsequently decreased. The crystallization of ZnO during the hydrothermal process is expected to play an instrumental role for the defect characteristics. The strain properties of ZnO nanostructures in response to the change in these nanostructures were investigated through high-resolution X-ray diffraction (HRXRD) and temperature-dependent PL spectra. Measurements were performed to examine the structural and optical properties of the ZnO nanostructures.

For the temperature-dependent PL measurements, samples were mounted in a closed-cycle He cryostat, then excited by a continuous-wave He–Cd laser, covering a wide temperature range from 20 to 300 K. The yellow–orange emission was attributed to the excess oxygen vacancies in the ZnO nanostructures. The temperature dependence of the PL peak energy was shown to fit a Gaussian distribution. The surface morphology was also examined by the scanning electron microscopy (SEM). Images were taken with a JSM-7500F instrument, as shown in our previous report [30,31].

3. Results and discussion

The X-ray diffraction (XRD) peak profiles of the samples investigated are shown in Fig. 1(a). The diffraction peaks from the nanocrystallite responses have a wurtzite hexagonal ZnO structure with a (0 0 2) preferred orientation and the narrow broadenings indicate good crystallinity of the as-synthesized products. The distinct diffraction of the hexagonal wurtzite ZnO with lattice constants of $a=b=0.3249$ nm and $c=0.5206$ nm can be indexed as corresponding to the crystal planes of ZnO (1 0 0), ZnO (1 0 1), ZnO (1 0 2), and ZnO (1 0 3), respectively, while the diffraction peak located at 29.6 corresponds to Si (1 1 1). Moreover, as shown in Fig. 1(b), lattice parameters of 2.858, 2.857, and 2.855 were obtained for S1, S2, and S3 respectively by extrapolating the

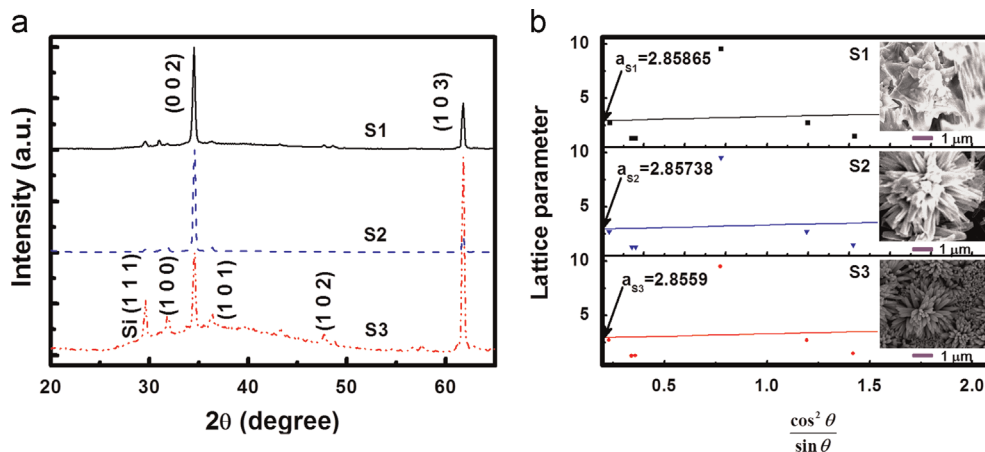


Fig. 1. (a) X-ray diffraction pattern and (b) lattice parameters of the ZnO nanostructures grown on Si substrates.

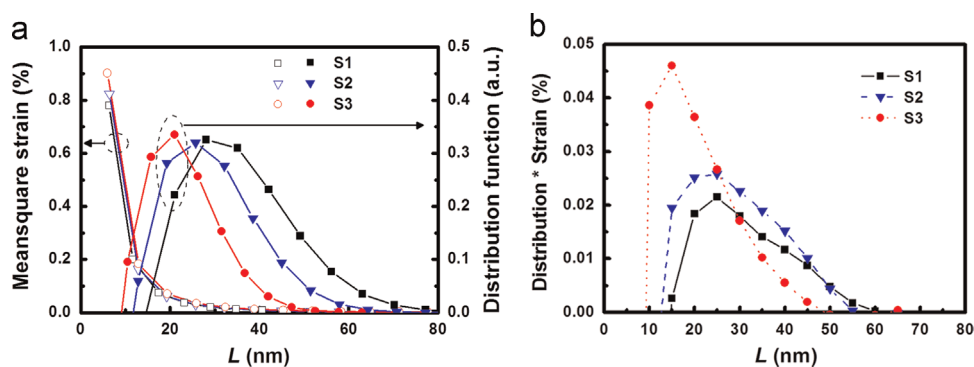


Fig. 2. (a) The size distribution and root-mean-square of the average strain as a function of column length for the ZnO nanostructure; (b) average lattice strain of the ZnO nanostructure derived from statistical approach.

straight lines of the parameter versus the 48.6 extrapolation function of the diffraction angle to the value corresponding to zero [32]. These results can be attributed to disordering and incoherence in the nano-ZnO arrangements associated with multiple reflections in the high angle region of the diffraction spectra [33]. The insubstantial difference of the lattice parameters among the three samples was inescapable, indicating that the variation of nanolattice strain originating from atomic bond strength changes during the hydrothermal reactions [32–34]. To determine more intrinsic features of the nanostructures, including the nanocrystallite size distribution and the strain profile functions, the XRD spectra were analyzed by using the Warren–Averbach method in Fourier space. Fig. 2(a) indicates the distribution of nanocrystallite sizes and the mean-square strains for the ZnO nanostructures [35–37]. The size distributions are essentially given by the so-called chord-length distribution function, attributed to random crystallization [38]. Examination of the lattice parameters for the three samples presented in Fig. 1(b) shows a clear correlation, with the increase in crystallite size associated with a reduction in the lattice parameters and vice versa, which is consistent with the SEM observations. There have been many reports of the extension of the lattice with decreasing particle size [39–41]. Inset of Fig. 1(b) shows the SEM images of the ZnO nanostructures grown on the Si substrate. The SEM images of ZnO nanostructures from sample 1 to sample 3 reveal decreases in the size of nanostructures. The growth parameters control the diameters and length of the nanostructures such as NH_4OH concentration. The morphology of crystals must be a result of synergism between the internal structure and the experimental conditions. Lattice strain was observed to decrease with an increase in the particle size. Different surface to volume ratios of nanostructures with different diameters may affect the intensities of the defect

emissions. It has also been observed that the mean-square strain in all samples decreases monotonically with increasing nano-ZnO sizes. The results are shown in Fig. 2(a). It can be seen in Fig. 2(b) that the average lattice strain obtained with the statistical approach was 0.917%, 0.964% and 1.348% for S1, S2, and S3, respectively, i.e.

$$\varepsilon_a = \frac{\int_0^{45} A_{\text{size}} \cdot A_{\text{strain}} dL}{\int_0^{45} dL}, \quad (1)$$

where ε_a is the average lattice strain, A_{strain} is the mean square strain, A_{size} is the size distribution function, and L is the crystallite size. Analysis of built-in strain and synthesized lattice nanostructure characteristics revealed that the lattice strain was a function of both the lattice parameter and of the particle size. According to the SEM images, it was found that the strain stored in the crystalline increased with a decrease in the nanoparticle size. The XRD analysis showed an increase in the lattice strain and the concentration of NH_4OH in ZnO nanostructures as a function of the particle size. The increase in the lattice parameter of ZnO nanostructures with decreasing particle size was attributed to the lattice strain induced by the creation of defect in the ZnO nanostructures [39–41]. According to the crystal field theory, it is expected that defect luminescence can be engineered by application of local strain through incoherent hetero-formation in nanostructures [28]. Our results showed that samples with satisfactory built-in strain were achieved using the hydrothermal method, providing a methodological basis not only for optical characterization, but also for analytical investigation.

In order to obtain further insight into the thermal-related strain effect of defect luminescence, PL measurements were carried out. Normalized PL spectra at 20 K for all three samples are shown in Fig. 3.

There were three PL peaks around 2.0 eV, 3.1 eV, and 3.5 eV, respectively, similar to the observations in nano-ZnO grown on Si, ITO, and sapphire [13,16,42]. The considerably stronger deep level emission in the green region was assigned to the oxygen vacancy-related transition. Accordingly, since high ammonia concentration facilitates the oxygen vacancy defects formed in ZnO nanostructures, it has been found that defect luminescence radiates from oxygen vacancy, as expected. The purple and ultraviolet emissions were attributed to Zinc interstitial (Zn_i), and near-band edge (NBE) excitons in interband recombinations, respectively. Correspondingly, the size variation of the structural imperfections formed in ZnO nanostructures exhibited a broad full width at half-maximum (FWHM) of 69.0 meV, while the FWHM for the excitons was 61.7 meV and 59.5 meV.

In Fig. 4, we calculated the correlation between PL spectrum and strain in S1 to S3 according to the three-energy different defects of PL spectrum for recombination processes. The dashed line is the Wei et al. curve for the set of parameters given in the report [43]. The S1 to S3 emissions were observed to exhibit different defects dependences as the strain was increased from S1 to S3. The excitation-dependent shifts of the S1 to S3 emissions are illustrated in deformation potential theory using a simple model strain energy \propto strain volume, where strain energy is the photon energy of PL spectrum. Fig. 4 reveals that the photon energy of PL spectrum shows a strong dependence on strain, while the different defects of spectrum exhibit relationship with the strain.

The temperature dependences of the photon emissions arising from the defects and excitons are illustrated in Fig. 5(a) and (b), respectively. The expected changes of the defect luminescence were evident at 37.24 meV, 48.24 meV, and 116.2 meV for S1, S2, and S3, respectively, over a broad temperature range from 20 to 300 K, while the temperature-insensitive spectral energies of both Zn_i and NBE emissions were observed. The marked difference in optical characteristics was commonly believed to attribute to different transition processes [44]. Many controversial arguments on

the origins of the temperature-dependent shifts of these three emissions have been proposed [45]. Generally, according to the well-developed deformation potential theory and the Varshni semiempirical relation, the redshifted exciton emission is attributed to temperature-induced bandgap shrinkage [1]. However, the blueshift of the defect luminescence is a result of temperature-related transitions between the band edge and the deep levels [20]. Obviously, from the reports so far, the thermal-induced nanolattice dilations play an inescapable role in the changes in spectral behavior with temperature for nanostructured ZnO. However, the realistic electronic structures are very delicate; it is believed that the extension of the localized excitonic states due to oxygen vacancies surrounded by positively charged ions has the relatively immense dimensions in the range from 10^{-7} to 10^{-6} cm [46]. Since the actual calculation of the energy levels is considerably more complex for given defects, the temperature-dependent characteristics must be assessed by the single-electron Hamiltonian assuming that the transition energies of the deep levels do not vary appreciably with the band edges [47–49].

Assuming that the potential well of the defects is thermally distorted from a cube into a parallelepiped, the change in the ground band energy is governed by

$$\Delta E(\epsilon) = E(T + \Delta T) - E(T) = \frac{\hbar^2 \pi^2}{2m^* a^2} \left[2(\epsilon + 1)^{-2} + (\epsilon + 1)^4 \right], \quad (2)$$

where a is the localized excitonic radius, m^* is the effective mass, and $E(T)$ is the energy of the green emission at the temperature of T [50]. As far as the thermal strain-induced spectral shifts are concerned, the shifts in defect luminescent are modulated by the lattice nano-strain of $\epsilon = \frac{a_{Si}(1 - \beta_{Si}T) - a_{ZnO}(1 - \beta_{ZnO}T)}{a_{ZnO}(1 - \beta_{ZnO}T)}$, where a_{Si} and a_{ZnO} are the lattice constants for Si and ZnO, respectively; and β_{Si} and β_{ZnO} are the coefficients of thermal expansion (CTE) of Si and ZnO, respectively. As we know, in relation to the size effect on the CTE, large crystallite sizes are associated with low thermal expansion, small sizes with high expansion [51,52]. Based on the observations in Figs. 1 and 2, the CTE values are 3.34×10^{-6} , 3.29×10^{-6} , and 2.9×10^{-6} for S1, S2, and S3, respectively, as estimated to obtain the best fit of the experimental data using Eq. (1), as shown by the dotted lines in Fig. 5(a). It was found that the blueshifts in the emission peaks were modulated by the tensile strain built in the nano-ZnO with increasing temperatures, clearly reflecting the smaller lattice constant and the smaller CTE of the deposited ZnO as compared with those of the Si substrates. Several similar reports have revealed that the tensile strain is responsible for changes in the optical properties in ZnO nanostructures [53]. The analytical results were corroborated by a similar attempt to evaluate the internal strain dependence of the interband transition energy subject to tensile strain. Based on the effective-mass Hamiltonian derived from the k.p method for wurtzite structures, band edge shifts caused by the thermal-induced tensile strain can be described using the deformation potential theory as

$$\Delta E = 2 \left[(a_{cz} - D_1 - D_3) \left(-\frac{C_{13}}{C_{33}} \right) + (a_{cz} - D_2 - D_4) \right] (\epsilon_{xx} - \epsilon_{yy}), \quad (3)$$

where $a_{cz} = 1.23$ and $a_{cz} = -0.68$ are the lattice constants of ZnO in the growth direction and the in-plane, respectively; $C_{13} = 105$ and $C_{33} = 211$ are the stiffness constants of ZnO; $D_1 = -3.06$, $D_2 = -2.46$, $D_3 = -0.47$, and $D_4 = 0.84$ are the deformation potential coefficients of ZnO; and $\epsilon_{xx} = 0.670769$ and $\epsilon_{yy} = 0.671776$ are the in-plane tensile strains, as mentioned above [54]. The obtained numerical results are plotted as the dashed line in Fig. 5(b). The redshift was close to zero as the temperature increased from 20 K to 300 K, which is consistent with the thermal insensitivity of band emissions compared to the defect emission. The results are essential not only for defect engineering, but also for strain engineering in semiconductor technology.

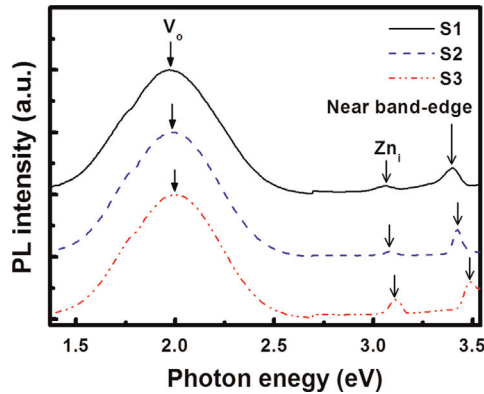


Fig. 3. Low-temperature photoluminescence spectra of the ZnO nanostructures.

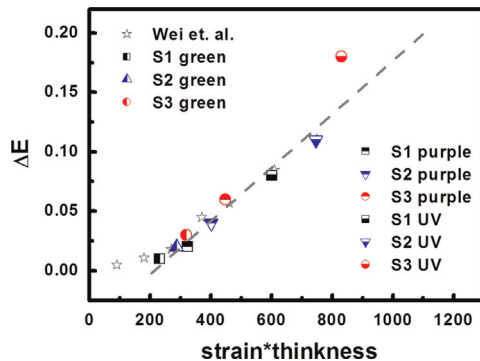


Fig. 4. The shift of photon energy versus strain*thickness curves.

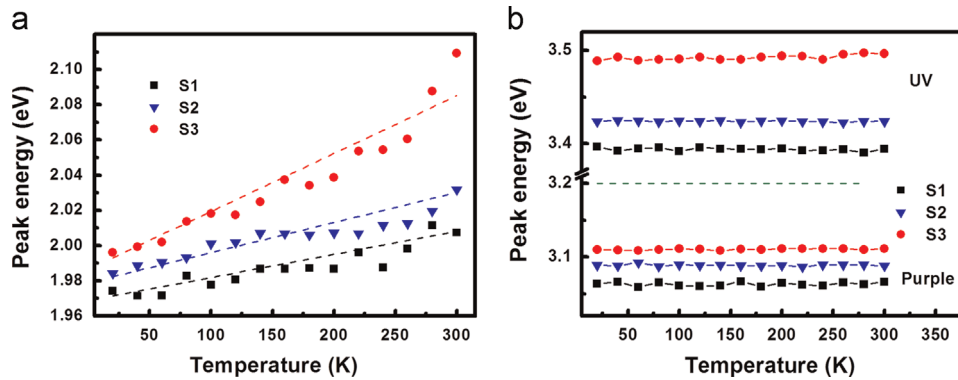


Fig. 5. Temperature dependence of the (a) green emission energy and (b) purple emission energy and UV emission energy for the ZnO nanostructures.

4. Conclusions

The effects of strain on modulating defect-related green luminescence from ZnO nanostructures grown on Si substrates have been investigated in-depth by careful adjustment of the aqueous solution of $\text{Zn}(\text{NO}_3)_2$ and NH_3OH used in the hydrothermal method. Well-ordered nano-size ZnO with different amounts of internal strain and average crystallite size distribution was subtly realized from Warren–Averbach Fourier analysis of the X-ray diffraction profiles. We report the controlled variation of luminescence of ZnO nanostructures from intense ultraviolet to bright visible light. Using temperature-dependent photoluminescence measurements over a broad temperature range from 20 to 300 K we discussed the oxygen vacancy-related and band-to-band emissions characterization. The difference in the thermal expansion between the ZnO crystallites and the Si substrate affected the blueshift of the green emission with increasing temperature. The violet and ultraviolet emissions were thermally insensitive that attributed to the thermal-related tensile strain. The deformation potential theory substantially corroborated the spectral observations indicating that modulation of the defect luminescence based on tensile strain in nano-ZnO had been successfully achieved in response to the difference in the thermal expansion between the ZnO crystallites and the Si substrate.

Acknowledgments

The authors would like to acknowledge support from the staff of GALOIS (Group of Abel and Lie Operations In Sciences) and the QUEST Laboratory (Quantum Electro-optical Science and Technology Laboratory), as well as the Graduate Institute of Electro-Optical Engineering and Department of Electronic Engineering, Chang Gung University, Taiwan. This study was financially supported by the Ministry of Science and Technology, ROC under Contract no. MOST 103-2112-M-182-001 and 104-2112-M-182-002.

References

- [1] H. Zeng, G. Duan, Y. Li, S. Yang, X. Xu, W. Cai, *Adv. Funct. Mater.* 20 (2010) 561.
- [2] X. Zhang, J. Qin, Y. Xue, P. Yu, B. Zhang, L. Wang, R. Liu, *Sci. Rep.* 4 (2014) 4596.
- [3] M.J.S. Spencer, *Prog. Mater. Sci.* 57 (2012) 437.
- [4] G.R. Li, T. Hu, G.L. Pan, T.Y. Yan, X.P. Gao, H.Y. Zhu, *J. Phys. Chem. C* 112 (2008) 11859.
- [5] D. Chu, Y. Masuda, T. Ohji, K. Kato, *Langmuir* 26 (2010) 2811.
- [6] Y. Darici, P.H. Holloway, J. Sebastian, T. Trottier, S. Jones, J. Rodriguez, *J. Vac. Sci. Technol. A* 17 (1999) 692.
- [7] E.M. Likovich, R. Jaramillo, K.J. Russell, S. Ramanathan, V. Narayanamurti, *Appl. Phys. Lett.* 99 (2011) 151910.
- [8] C. Ton-That, L. Weston, M.R. Phillips, *Phys. Rev. B* 86 (2012) 115205.
- [9] J.Y. Park, D.J. Lee, Y.S. Yun, J.H. Moon, B.T. Lee, S.S. Kim, *J. Cryst. Growth* 276 (2005) 158.
- [10] S.H. Jeong, E.S. Aydil, *J. Cryst. Growth* 311 (2009) 4188.
- [11] M. Willander, O. Nur, J.R. Sadaf, M.I. Qadir, S. Zaman, A. Zainelabdin, N. Bano, I. Hussain, *Materials* 3 (2010) 2643.
- [12] E. Gür, S. Tüzemen, K. Meral, Y. Onganer, *Appl. Phys. A* 94 (2009) 549.
- [13] B. Lin, Z. Fu, Y. Jia, *Appl. Phys. Lett.* 79 (2001) 943.
- [14] S. Al-lami, H. Jaber, *Chem. Mater. Res.* 6 (2014) 101.
- [15] S. Baruah, J. Dutta, *Sci. Technol. Adv. Mater.* 10 (2009) 013001.
- [16] N.H. Alvi, K. Hasan, O. Nur, M. Willander, *Nanoscale Res. Lett.* 6 (2011) 130.
- [17] S. Lin, H. Hu, W. Zheng, Y. Qu, F. Lai, *Nanoscale Res. Lett.* 8 (2013) 158.
- [18] A. Ismail, M.J. Abdullah, *J. King Saud Univ.—Sci.* 25 (2013) 209.
- [19] B. Lin, Z. Fu, Y. Jia, G. Liao, *J. Electrochem. Soc.* 148 (2001) G110.
- [20] Y.H. Chang, S.M. Wang, C.M. Liu, C. Chen, *J. Electrochem. Soc.* 157 (2010) K236.
- [21] N.S. Norberg, D.R. Gamelin, *J. Phys. Chem. B* 109 (2005) 20810.
- [22] K. Mahmood, S.B. Park, H.J. Sung, *J. Phys. Chem. C* 1 (2013) 3138.
- [23] C.K. Xu, P. Shin, L.L. Cao, D. Gao, *J. Phys. Chem. C* 114 (2010) 125.
- [24] S.B. Zhang, J.E. Northrup, *Phys. Rev. Lett.* 67 (1991) 2339.
- [25] D.B. Laks, C.G. Van de Walle, G.F. Neumark, S.T. Pantelides, *Phys. Rev. Lett.* 66 (1991) 648.
- [26] C.G.V. d. Walle, J. Neugebauer, *J. Appl. Phys.* 95 (2004) 3851.
- [27] A. Janotti, C.G.V. d. Walle, *Rep. Prog. Phys.* 72 (2009) 126501.
- [28] Q. Yang, W. Wang, S. Xu, Z.L. Wang, *Nano Lett.* 11 (2011) 4012.
- [29] P.A. Leighton, *J. Chem. Educ.* 18 (1941) 249.
- [30] J.C. Wang, F.C. Cheng, Y.T. Liang, H.I. Chen, C.Y. Tsai, C.H. Fang, T.E. Nee, *Nanoscale Res. Lett.* 7 (2012) 270.
- [31] J.C. Wang, Y.T. Liang, F.C. Cheng, C.H. Fang, H.I. Chen, C.Y. Tsai, J.A. Jiang, T. E. Nee, *J. Lumin.* 136 (2013) 11.
- [32] F. Karsai, P. Tiwald, R. Laskowski, F. Tran, D. Koller, S. Grafe, J. Burgdorfer, L. Wirtz, P. Blaha, *Phys. Rev. B* 89 (2014) 125429.
- [33] R. Kumar, G. Sharma, M. Kumar, *Mod. Phys. Lett. B* 27 (2013) 1350180.
- [34] D. Shiri, A. Verma, C.R. Selvakumar, M.P. Anantram, *Sci. Rep.* 2 (2012) 461.
- [35] B.E. Warren, B.L. Averbach, *J. Appl. Phys.* 21 (1950) 595.
- [36] B.E. Warren, B.L. Averbach, *J. Appl. Phys.* 23 (1952) 497.
- [37] K. Reimann, R. Würschum, *J. Appl. Phys.* 81 (1997) 7186.
- [38] A.P. Roberts, S. Torquato, *Phys. Rev. E* 59 (1999) 4953.
- [39] S. Deshpande, S. Patil, S. VNT Kuchibhatla, S. Seal, *Appl. Phys. Lett.* 87 (2005) 133113.
- [40] X.D. Zhou, W. Huebner, *Appl. Phys. Lett.* 79 (2001) 3512.
- [41] S. Tsunekawa, S. Ito, Y. Kawazoe, *Appl. Phys. Lett.* 85 (2004) 3845.
- [42] M. Mekhnache, A. Drici, L.S. Hamideche, H. Benzarrouk, A. Amara, L. Cattin, J. C. Bernède, M. Guerionne, *Superlattices Microstruct.* 49 (2011) 510.
- [43] B. Wei, K. Zheng, Y. Ji, Y. Zhang, Z. Zhang, X. Han, *Nano Lett.* 12 (2012) 4595.
- [44] A.B. Djurisic, Y.H. Leung, *Small* 2 (2006) 944.
- [45] C. Chen, H. He, Y. Lu, K. Wu, Z. Ye, *ACS Appl. Mater. Interfaces* 5 (2013) 6354.
- [46] W. Kohn, *Solid State Phys.* 5 (1957) 257.
- [47] Y. Gong, T. Andelman, G.F. Neumark, S. O'Brien, I.L. Kuskovsky, *Nanoscale Res. Lett.* 2 (2007) 297.
- [48] T. Miyasaka, T.N. Murakami, *Appl. Phys. Lett.* 85 (2004) 3932.
- [49] A.L. Efros, M. Rosen, *Annu. Rev. Mater. Sci.* 30 (2000) 475.
- [50] J.L. Basdevant, J. Dalibard, *The Quantum Mechanics Solver : How to Apply Quantum Theory to Modern Physics*, Springer, Berlin, 2000.
- [51] S. Hwang, Y. Kim, *J. Nanosci. Nanotechnol.* 11 (2011) 1555.
- [52] I. Juárez-Ramírez, K. Matsumaru, K. Ishizaki, L.M. Torres-Martínez, *J. Ceram. Process. Res.* 9 (2008) 509.
- [53] R. Chen, Q.L. Ye, T.C. He, T. Wu, H.D. Sun, *Appl. Phys. Lett.* 98 (2011) 241916.
- [54] J.M. Wagner, F. Bechstedt, *Phys. Rev. B* 66 (2002) 115202.